Supporting information

Deciphering the role of Van der Waals heterostructures in enhancing layered perovskite anodes for high-performance lithium-ion batteries

Xiao-Hui Wu[1, #], Yun Chai[1, #], Jie Shen[3], Pei-Wen Huang[1], Si-Yu Xu[1], Hou-Yang Zhong[1], Bi-Cui Chen[1], Yi Zhao[2, *], Baisheng Sa[3, *], and Ke-Zhao Du[1, *]

[1]College of Chemistry and Materials Science, Fujian Provincial Key Laboratory of Advanced Materials Oriented Chemical Engineering, Fujian Normal University, Fuzhou, 350117, China

[2]Strait Institute of Flexible Electronics (SIFE Future Technologies), Fujian Key Laboratory of Flexible Electronics, Fujian Normal University and Strait Laboratory of Flexible Electronics (SLoFE), Fuzhou 350117, China

[3]Multiscale Computational Materials Facility & Materials Genome Institute, School of Materials Science and Engineering, Fuzhou University, Fuzhou 350100, China

[#] These authors contributed equally to this work.

[*]Corresponding author

E-mail: duke@fjnu.edu.cn; ifeyzhao@fjnu.edu.cn; bssa@fzu.edu.cn

Materials Synthesis

Synthesis of $Li_2(taurine)_2CuCl_4$ (LTCC)

Taurine (99%, Macklin), Copper (II) chloride, anhydrous ($CuCl_2$, 97%, Acros), Lithium chloride, anhydrous (LiCl, 99%, Adamas). All chemicals were directly used without further purification. For the fabrication of LTCC, taurine (75 mg, 0.60 mmol) and anhydrous $CuCl_2$ (0.30 mmol) were added to a 10 M LiCl aqueous solution (0.3 ml) in a 4 mL vial. The mixture was heated to 100 °C and stirred until the precursors were completely dissolved. Then, the vial was left to cool for 2–3 h and square yellow plate-like crystals precipitated.

Materials Characterization

The crystalline phase of as-prepared samples was characterized using a powder X-ray diffractometer (PXRD, Bruker D8 Advance) with Cu Kα radiation (λ = 1.5418 Å). The structure and composition of as-prepared samples were characterized by scanning electron microscopy (SEM, Hitachi SU8100) equipped with energy dispersive X-ray spectroscopy (EDS) and transmission electron microscopy (TEM, JEM F200). The chemical compositions and the bonding structures were determined by X-ray photoelectron spectroscopy (XPS, Thermo ESCALAB 250XI).

Electrochemical Measurements

The electrochemical properties were measured using coin cells (CR2032), where 1 M $LiPF_6$ solution in a mixture of ethylene carbonate, diethyl carbonate, and dimethyl carbonate (1:1:1 in volume) with 5.0 wt.% weight ratio fluoroethylene carbonate was used as the electrolyte, Celgard 2300 microporous membrane was used as separators, and lithium foil was used as the counter electrodes. The active materials, Ketjen black and polyvinylidene difluoride with a

weight ratio of 8: 1: 1, were mixed in N-methyl pyrrolidone. The slurry was placed onto copper foil to prepare the working electrode and dried at 80 °C for 12 h. The active material loading on the electrode (diameter was 12 mm) was 1-1.2 mg cm^{-2}. To assemble the CR2032-type coin cells, the argon atmosphere glove box (Mikrouna) was used, where both H_2O and O_2 were kept below 0.01 ppm. The galvanostatic charge/discharge tests in the voltage range of 0.005-3.0 V (vs. Li/Li^+) were performed with a LAND cycler test system at 30 °C. The cyclic voltammetry (CV) and electrochemical impedance spectroscopy (EIS, at the frequency range of 0.1 HZ to 100000 Hz) were measured on an electrochemical workstation (CHI660E, CH instrument).

Computational details

All calculations were performed using the PWmat code[1,2] with the norm-conserving SG15 pseudopotential.[3,4] The exchange-correlation interactions were treated by the generalized gradient approximation in the form of the Perdew–Burke–Ernzerhof (PBE) functional.[5,6] All calculations were also performed by including the Grimme dispersion corrections (DFT-D3).[7,8] To avoid the interactions between periodic images, a vacuum region > 15 Å was set along the direction perpendicular to the layer surface. The atom-surface distance was optimized by relaxing the first three layers of the slab. The energy cutoff of the plane-wave was set to 60 Ryd (~816.34 eV), and the maximum force convergence tolerances were set to 0.02 $eV \cdot Å^{-1}$. A 2 × 2 × 1 k-point sampling was used based on the Monkhorst-Pack scheme.[9] The nudged elastic band (NEB) method was used to optimize the Li atom migration paths and to evaluate the energy barriers associated with Li-ion diffusion on the material surface.

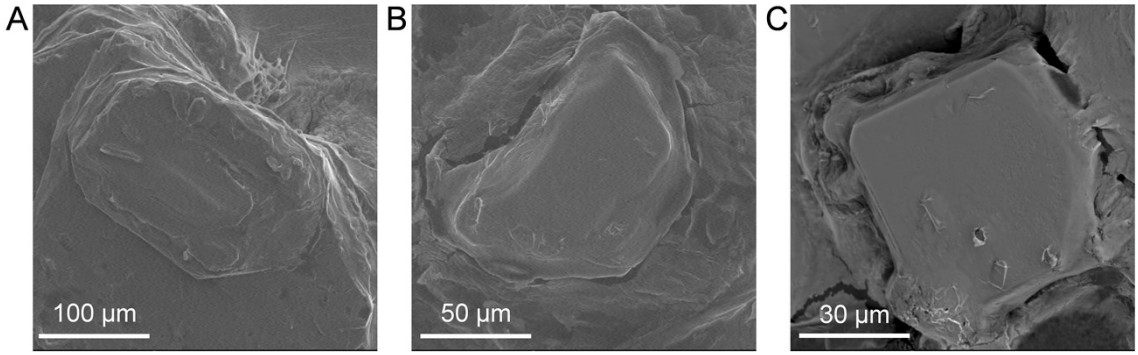

Fig. S1 (A-C) SEM images of LTCC crystals.

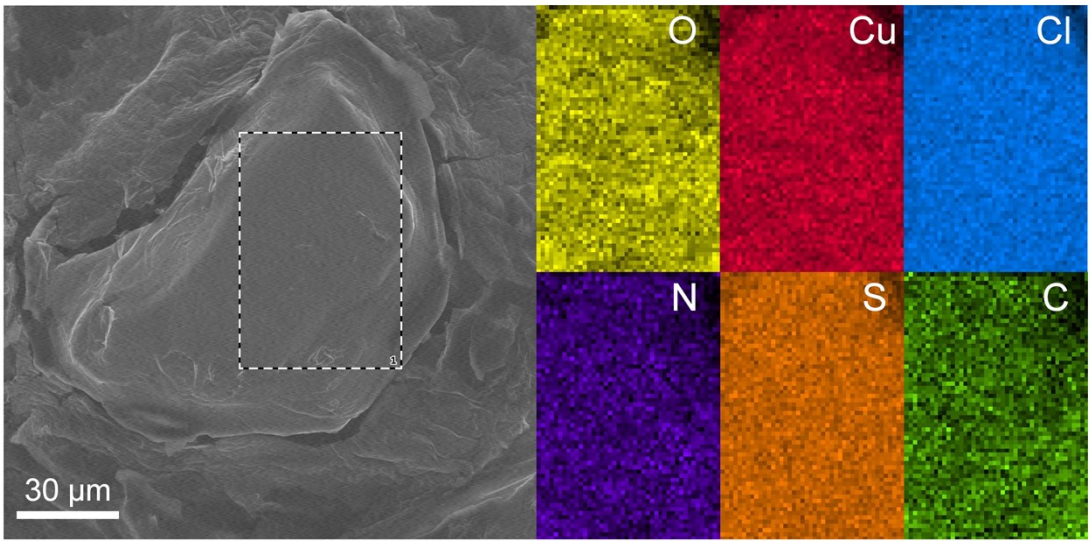

Fig. S2 SEM image with the corresponding EDS images of LTCC sample.

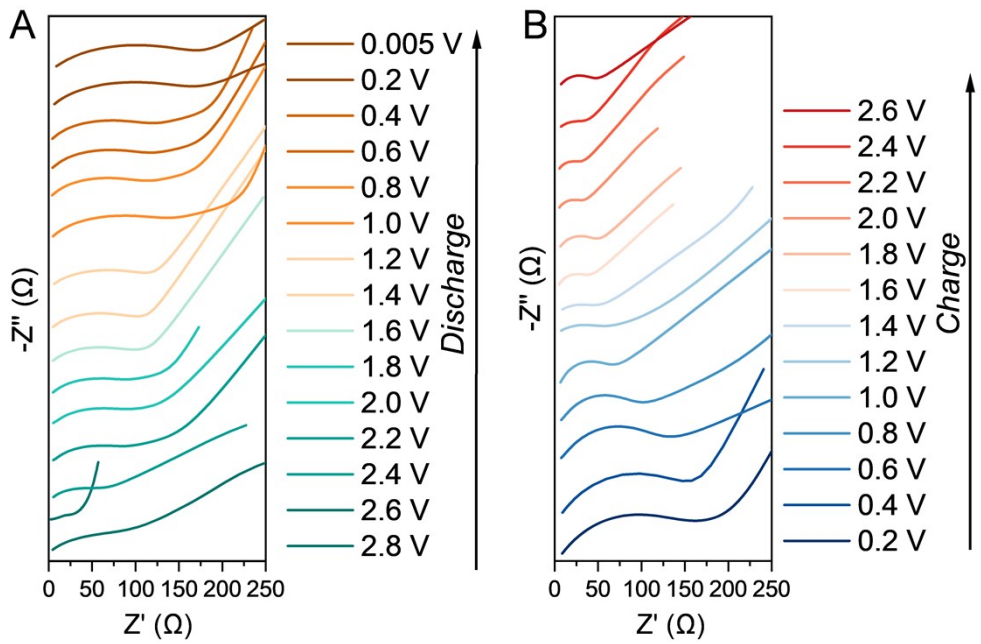

Fig. S3 The EIS spectra of the LTCC electrode at (A) different discharging voltages and (B) different charging voltages.

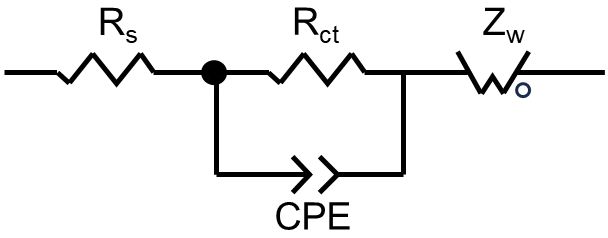

Fig. S4 The fitting equivalent circuit for EIS spectra.

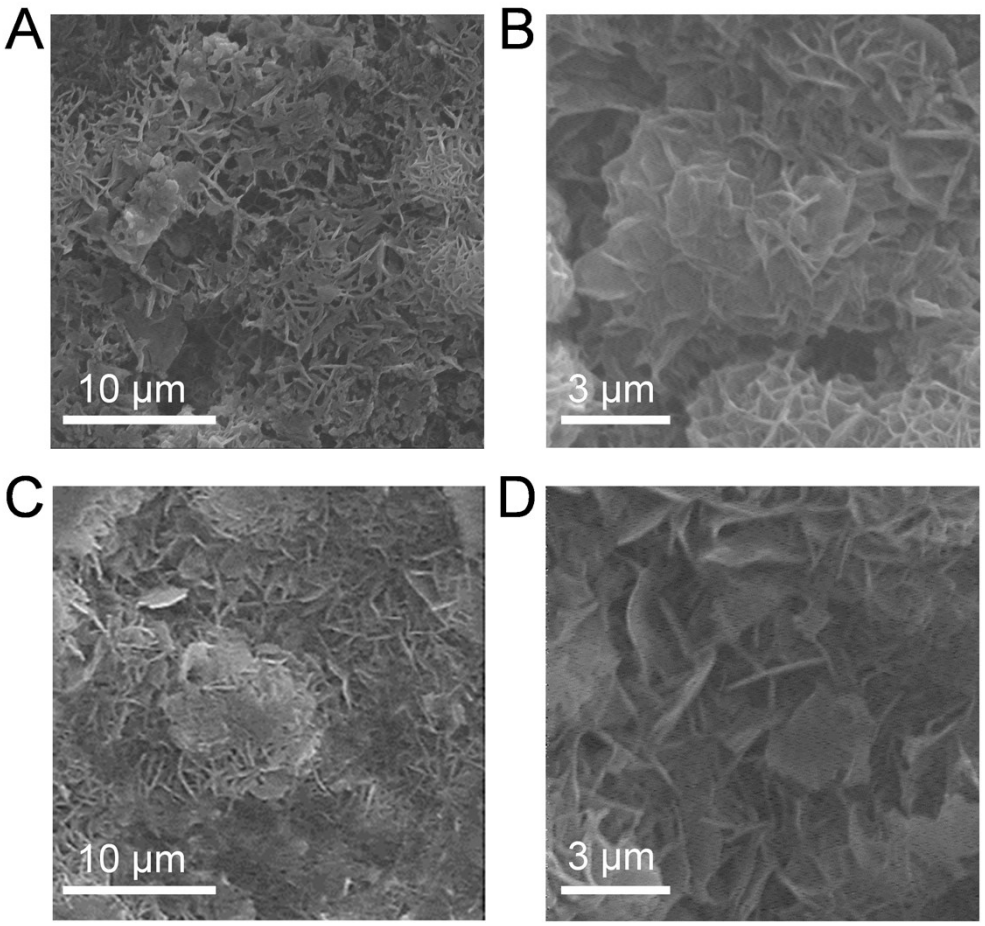

Fig. S5 SEM images of the LTCC electrode after (A-B) initial fully discharged state and (C-D) fully charged state.

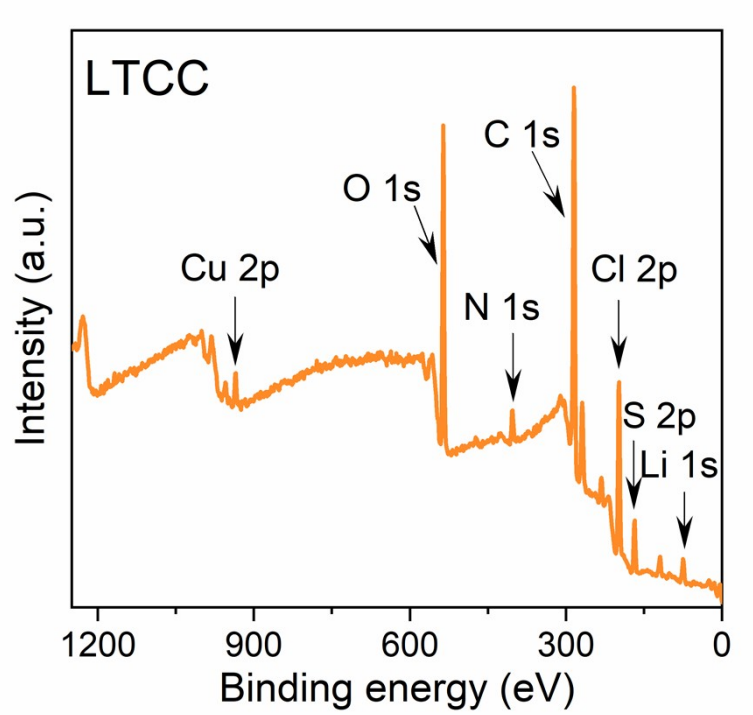

Fig. S6 XPS full survey of the fresh LTCC sample.

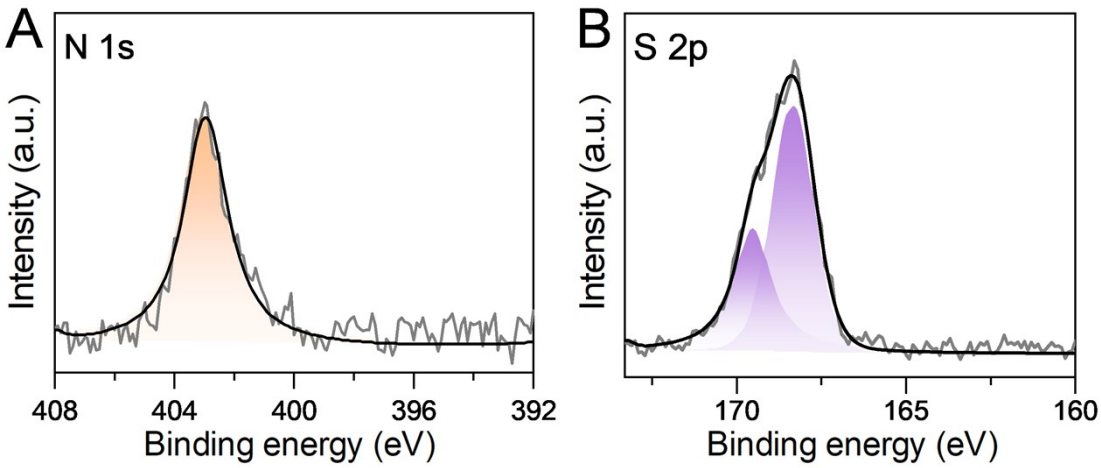

Fig. S7 High-resolution (A) N 1s and (B) S 2p XPS spectra of fresh LTCC.

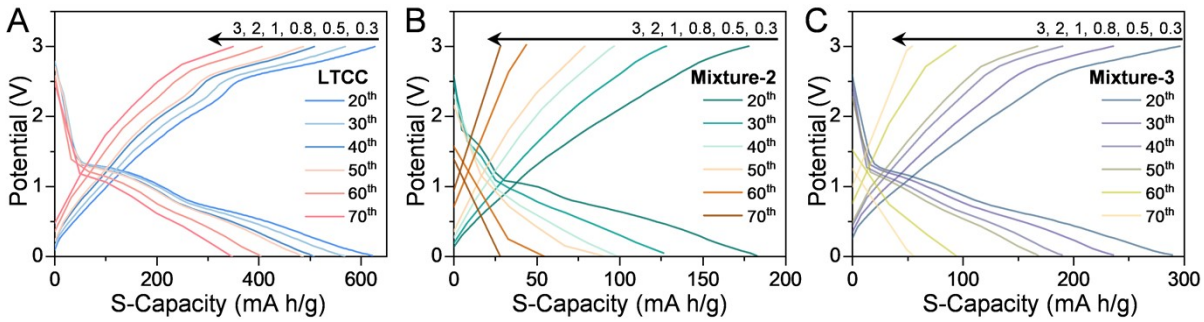

Fig. S8 Typical discharge/charge profiles under various current densities of (A) LTCC, (B) Mixture-2, and (C) Mixture-3 electrodes.

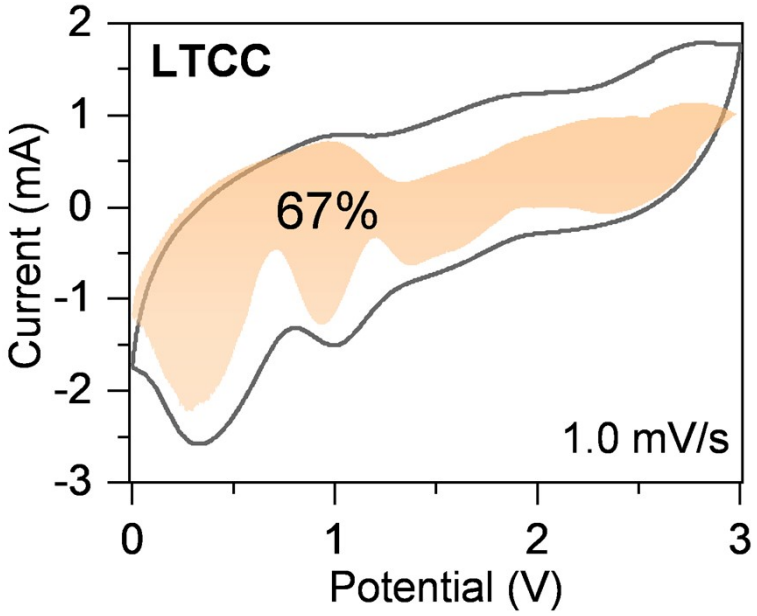

Fig. S9 Capacitive contribution during the lithiation/delithiation processes of LTCC electrode at at a scan rate of 1.0 mV/s.

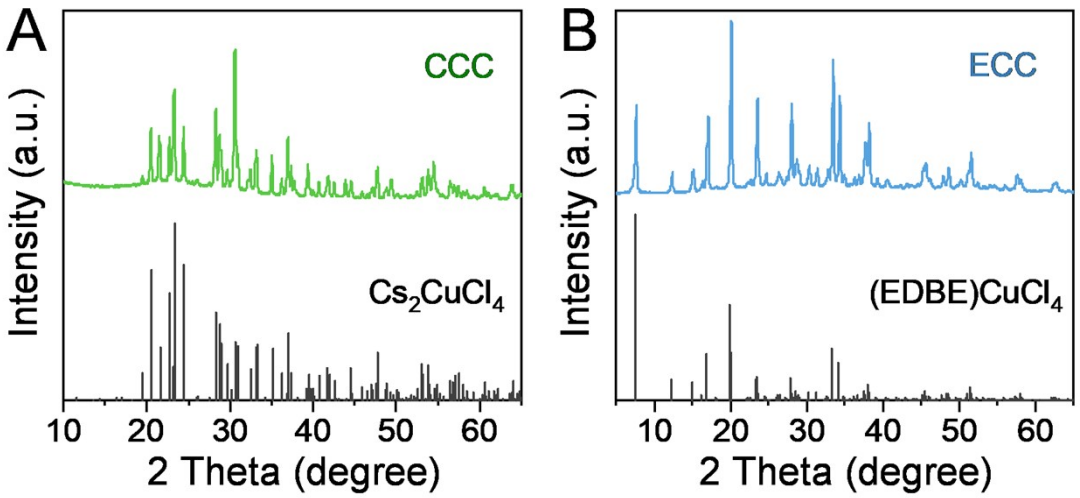

Fig. S10. The XRD patterns of the synthesized (A) CCC and (B) ECC crystals and the standard patterns of Cs_2CuCl_4 and (EDBE)$CuCl_4$.

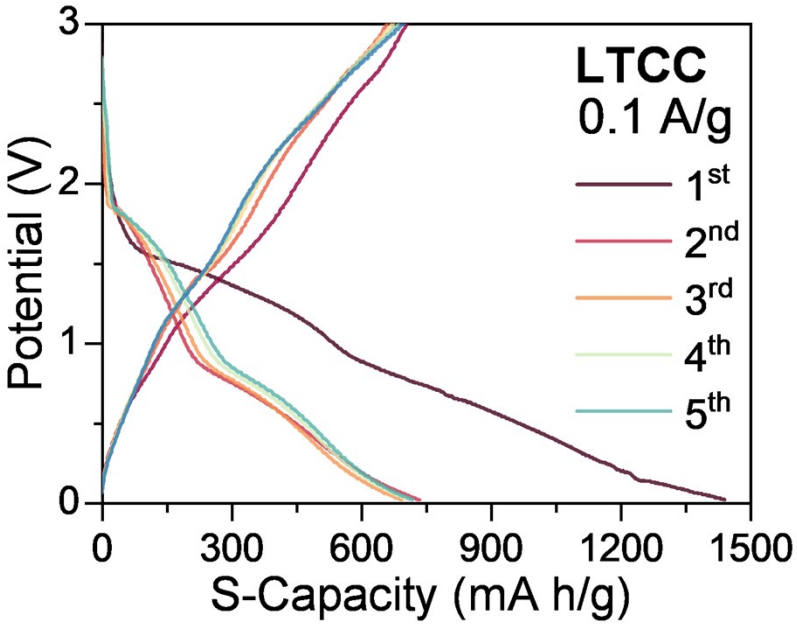

Fig. S11 GDC profiles of the LTCC electrode for the first five cycles at 0.1 A/g.

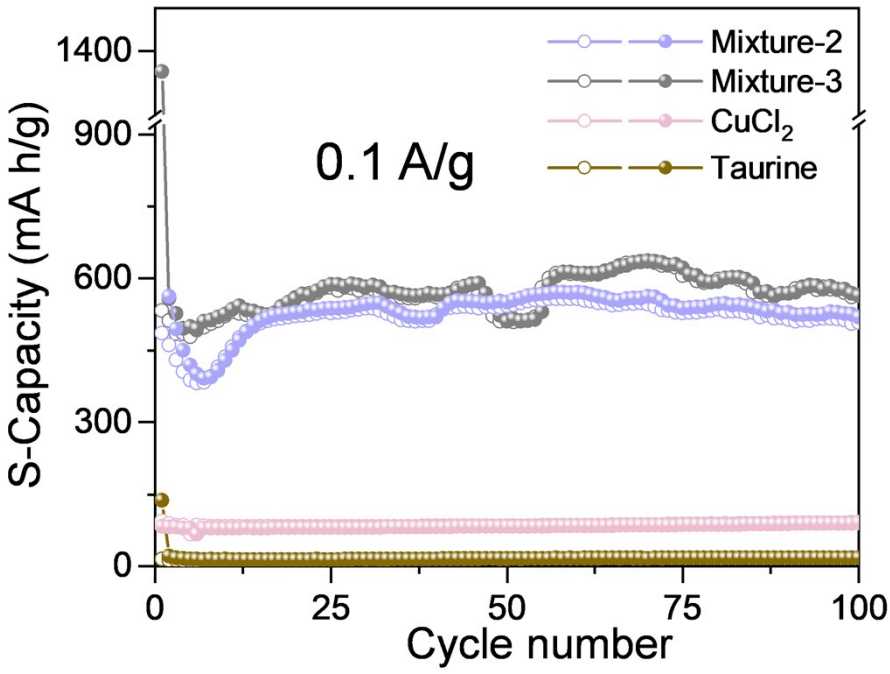

Fig. S12 Cycling performance of $CuCl_2$, Taurine, Mixture-2, and Mixture-3 electrodes at 0.1 A/g.

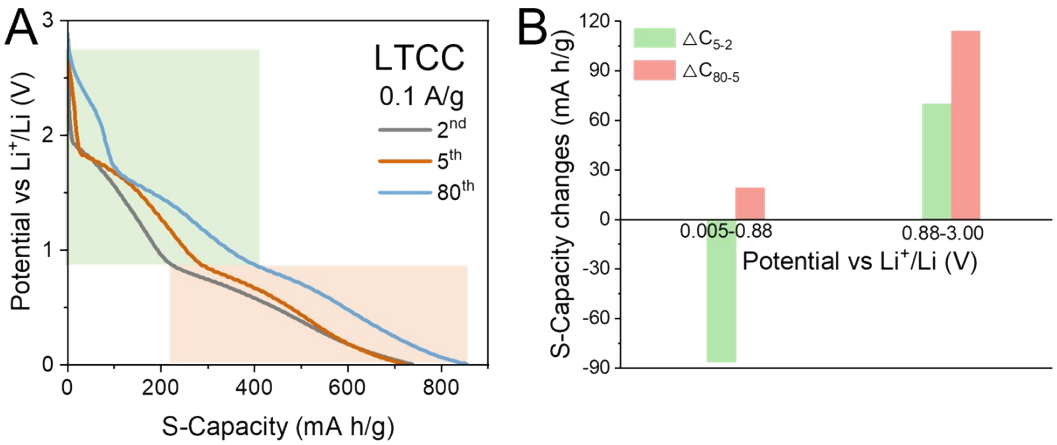

Fig. S13 (A) Comparison of the charge-discharge profiles at 2nd, 5th, and 80th cycles. (G) The calculated specific capacity in two potential regions of LTCC electrode at specified cycle numbers under 0.1 A/g in the range of 0.005-3.0 V.

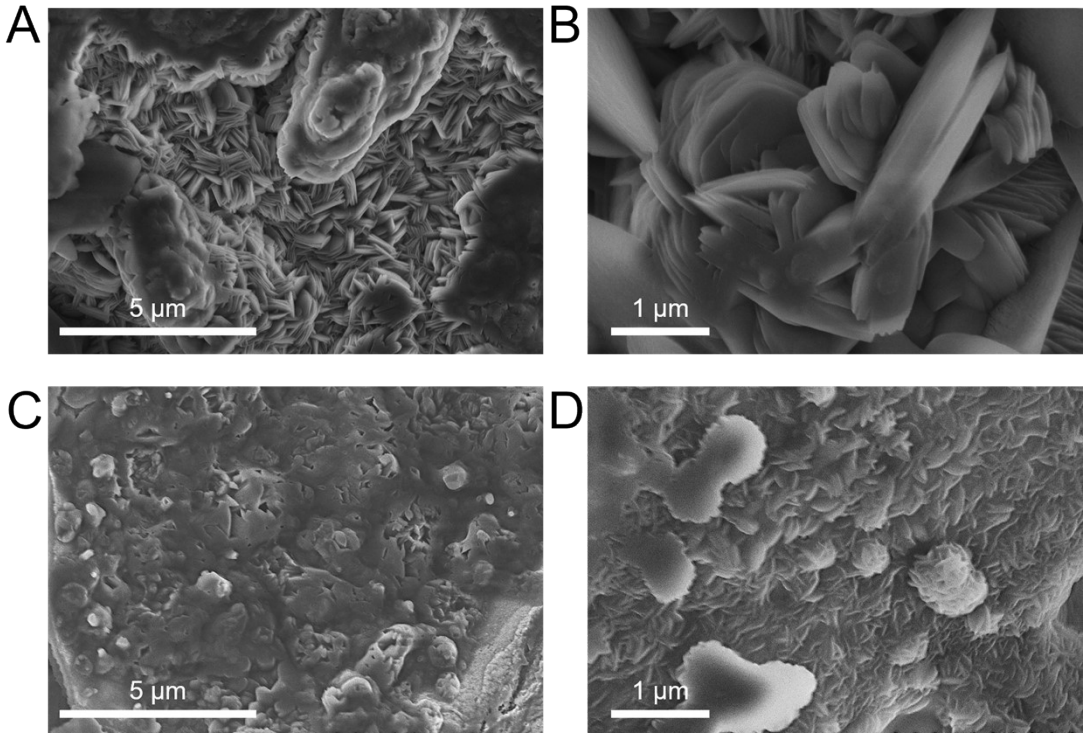

Fig. S14 SEM images of LTCC electrode at (A-B) the 5th cycle and (C-D) the 80th cycle.

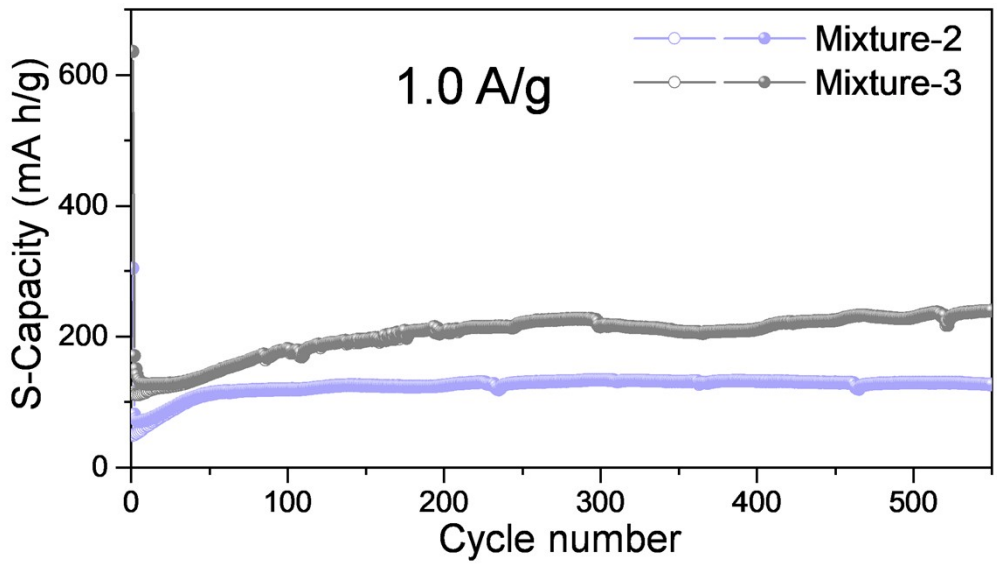

Fig. S15 Cycling performance of Mixture-2 and Mixture-3 electrodes at 1.0 A/g.

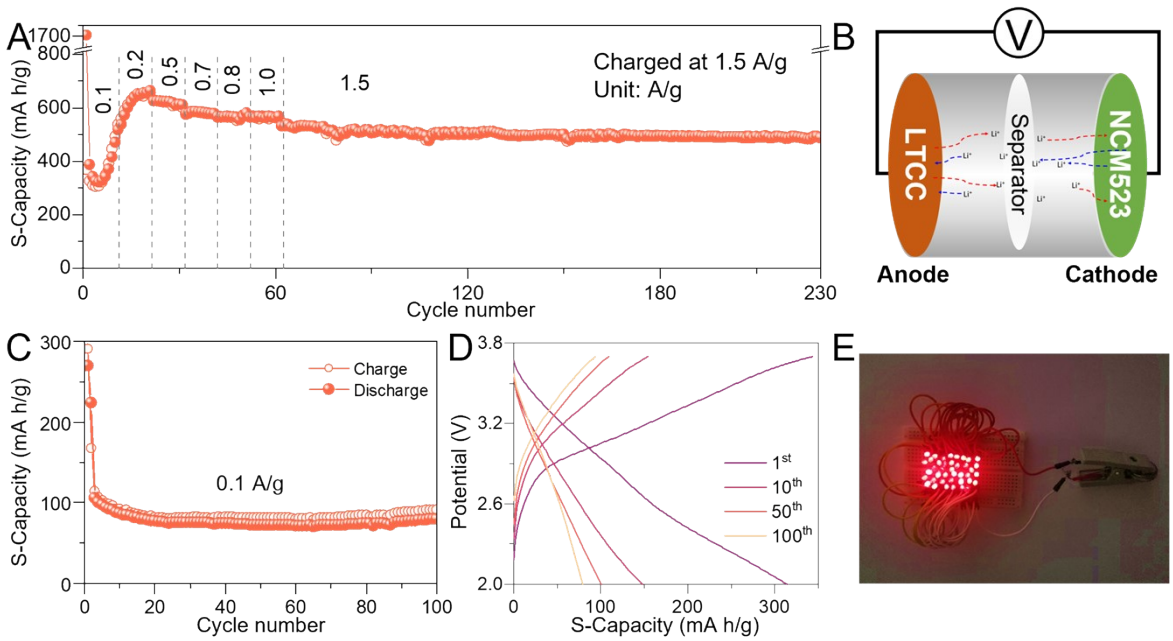

Fig. S16 (A) The fast charging and slow discharging performance of LTCC electrode. (B) A full battery with NCM523 as cathode and LTCC as anode. (C) Cycling performance and (D) the charge-discharge curves of LTCC II NCM523 full cell at 0.1 A/g. (E) 40 bright LEDs illuminated by a single LTCC II NCM523 full cell.

Table S1. Comparison of cycle performance of reported perovskite material and LTCC anode materials (The capacity calculation is based on the whole composite).

Materials	Cycling performance			Rate performance	References
	Current density (A/g)	Cycle Number	Specific capacity (mA h/g)		
LTCC	**0.1**	**100**	**870**	801, 490, and 380 mA h/g at 0.1, 1, and 3 A/g	**This work**
LTCC	**1.0**	**550**	**548**		**This work**
Cs_2CuBr_4/3D	0.5	200	415	390, 280, and 123 mA h/g at 0.1, 1, and 3 A/g	10
(EDBE)[$CuCl_4$]	0.028	200	52	No data	11
LiPCl	0.3	400	121	162, 114, and 117 mA h/g at 0.2, 0.5, and 1 A/g	12
2D Cu-THQ MOF	0.05	100	340	159 and 93 mA h/g at 0.5 and 1 A/g	13
$CeNb_3O_9$	0.05	200	195	195 and 103 mA h/g at 0.125 and 5 A/g	14
$[(Bi,Na)_{1/5}(La,Li)_{1/5}(Ce,K)_{1/5}Ca_{1/5}Sr_{1/5}]TiO_3$	1.0	300	120.4	87.4, 62, and 59.5 mA h/g at 0.1, 1, and 3 A/g	15
$HoFeO_3$	0.1	120	437	448, 408, and 365 mA h/g at 0.1, 1, and 3 A/g	16
$[C_2H_4N_3S][BiI_4]$	0.1	250	530	700, 240, and 200 mA h/g at 0.1, 1, and 2 A/g	17

Reference:

[1] Jia W, Fu J, Cao Z, et al., Journal of Computational Physics, 2013, 251: 102-115.

[2] Jia W, Cao Z, Wang L, et al., Computer Physics Communications, 2013, 184(1): 9-18.

[3] Schlipf M, Gygi F., Computer Physics Communications, 2015, 196: 36-44.

[4] D. R. Hamann, Physical Review B, 2013, 88: 085117.

[5] Perdew J P, Burke K, Ernzerhof M., Physical Review Letters, 1996, 77(18): 3865-3868.

[6] Perdew J P, Ernzerhof M, Burke K., The Journal of Chemical Physics, 1996, 105(22): 9982-9985.

[7] Grimme S, Antony J, Ehrlich S, et al., The Journal of Chemical Physics, 2010, 132(15): 154104.

[8] Grimme S, Journal of Computational Chemistry, 2006, 27(15): 1787-1799.

[9] Monkhorst H J, Pack J D., Physical Review B, 1976, 13(12): 5188-5192.

[10] Pandey, P.; Sharma, N.; Panchal, R. A.; Gosavi, S.; Ogale, S., ChemSusChem 2019, 12, 3742-3746.

[11] Jaffe, A.; Karunadasa, H. I., Inorganic Chemistry 2014, 53, 6494-6496.

[12] Lin, L.; Liang, F.; Zhang, K.; Mao, H.; Yang, J.; Qian, Y., Journal of Materials Chemistry A 2018, 6, 15859-15867.

[13] Jiang, Q.; Xiong, P.; Liu, J.; Xie, Z.; Wang, Q.; Yang, X. Q.; Hu, E.; Cao, Y.; Sun, J.; Xu, Y., Angewandte Chemie International Edition 2020, 59, 5273-5277.

[14] Yang, L.; Xiong, X.; Liang, G.; Li, X.; Wang, C.; You, W.; Zhao, X.; Liu, X.; Che, R., Advanced Materials 2022, 34, 2200914.

[15] Yan, J.; Wang, D.; Zhang, X.; Li, J.; Du, Q.; Liu, X.; Zhang, J.; Qi, X., Journal of Materials Science 2020, 55, 6942-6951.

[16] Nguyen, A. T.; Phung, V. D.; Mittova, V. O.; Ngo, H. D.; Vo, T. N.; Le Thi, M. L.; Mittova, I. Y.; Le, M. L. P.; Ahn, Y. N.; Kim, I. T., Scripta Materialia 2022, 207, 114259.

[17] Roy, K.; Li, T.; Ogale, S.; Robertson, N., Journal of Materials Chemistry A 2021, 9, 2689-2693.